

Buffer layer between a planar optical concentrator and a solar cell

Manuel E. Solano, Greg D. Barber, Akhlesh Lakhtakia, Muhammad Faryad, Peter B. Monk, and Thomas E. Mallouk

Citation: *AIP Advances* **5**, 097150 (2015); doi: 10.1063/1.4931386

View online: <http://dx.doi.org/10.1063/1.4931386>

View Table of Contents: <http://scitation.aip.org/content/aip/journal/adva/5/9?ver=pdfcov>

Published by the [AIP Publishing](#)

Articles you may be interested in

[Reducing optical and resistive losses in graded silicon-germanium buffer layers for silicon based tandem cells using step-cell design](#)

AIP Advances **5**, 057161 (2015); 10.1063/1.4921945

[Compound semiconductor solar cells on Si substrate for medium concentrator photovoltaic applications](#)

AIP Conf. Proc. **1556**, 101 (2013); 10.1063/1.4822209

[Effect of placing GaAs solar cells on the optical rod prism of a concentrated photovoltaic](#)

J. Renewable Sustainable Energy **5**, 043102 (2013); 10.1063/1.4812649

[A photovoltaic system with three solar cells and a band-stop optical filter](#)

J. Renewable Sustainable Energy **3**, 023113 (2011); 10.1063/1.3583506

[III-V junctions on silicon substrates using BeTe buffer layers for solar cell applications](#)

J. Appl. Phys. **103**, 064516 (2008); 10.1063/1.2891254

The advertisement features a large image of a water drop on the left, with ripples in the water. On the right, there is a smaller image of the journal cover for 'Computing - Science & Engineering'. The cover includes the title 'Computing - Science & Engineering', the subtitle 'Scientific Software Communities', and various icons representing different fields of study. To the right of the journal cover, there is text promoting the journal to scientists and engineers in 50+ societies, encouraging them to submit their computational articles to CISE.

Broaden your impact to scientists and engineers in 50+ societies. Submit your computational article to *CISE*.

Buffer layer between a planar optical concentrator and a solar cell

Manuel E. Solano,¹ Greg D. Barber,^{2,3} Akhlesh Lakhtakia,⁴
Muhammad Faryad,⁵ Peter B. Monk,⁶ and Thomas E. Mallouk³

¹*Departamento de Ingeniería Matemática and CI² MA, Universidad de Concepción, Concepción, Casilla 160-C, Chile*

²*Penn State Institute of Energy and the Environment, Pennsylvania State University, University Park, PA 16802, USA*

³*Department of Chemistry, Pennsylvania State University, University Park, PA 16802, USA*

⁴*Department of Engineering Science and Mechanics, Pennsylvania State University, University Park, PA 16802, USA*

⁵*Department of Physics, Lahore University of Management Sciences, Lahore 54792, Pakistan*

⁶*Department of Mathematical Sciences, University of Delaware, Newark, DE 19716, USA*

(Received 2 April 2015; accepted 7 September 2015; published online 15 September 2015)

The effect of inserting a buffer layer between a periodically multilayered isotropic dielectric (PMLID) material acting as a planar optical concentrator and a photovoltaic solar cell was theoretically investigated. The substitution of the photovoltaic material by a cheaper dielectric material in a large area of the structure could reduce the fabrication costs without significantly reducing the efficiency of the solar cell. Both crystalline silicon (c-Si) and gallium arsenide (GaAs) were considered as the photovoltaic material. We found that the buffer layer can act as an antireflection coating at the interface of the PMLID and the photovoltaic materials, and the structure increases the spectrally averaged electron-hole pair density by 36% for c-Si and 38% for GaAs compared to the structure without buffer layer. Numerical evidence indicates that the optimal structure is robust with respect to small changes in the grating profile. © 2015 Author(s). All article content, except where otherwise noted, is licensed under a Creative Commons Attribution 3.0 Unported License. [<http://dx.doi.org/10.1063/1.4931386>]

I. INTRODUCTION

Several authors have proposed to use a laminar dielectric structure called a planar optical concentrator (POC) to steer vertically incident solar light into a horizontal path towards photovoltaic solar cells mounted on the edges.¹⁻³ The substitution of the photovoltaic material by a cheaper dielectric material in a large area of the light-harvesting structure could reduce the fabrication costs without significantly reducing the efficiency of conversion of photonic energy into electrical energy. The large-area fabrication of such composite structures using patterning techniques such as soft lithography and particle assembly⁴⁻⁶ is now inexpensive enough that the concentrators and the photovoltaic components can have sub-mm dimensions. These micro-cell designs are forgiving with respect to the incorporation of optically lossy materials such as metals into the POC. They are also advantageous for heat dissipation, especially at the modest concentration ratios that are appropriate with relatively low-cost single-junction crystalline silicon (c-Si) and thin-film compound-semiconductor photovoltaic solar cells.

A POC comprising a periodic multilayered isotropic dielectric (PMLID) material backed by a metallic surface-relief grating was proposed and optimized earlier for c-Si solar cells.² The geometrical parameters and the refractive indexes of the materials in the POC were selected in order to maximize the solar-spectrum-integrated power-flux density inside the PMLID material. Consequently, the spectrally averaged electron-hole pair (EHP) density generated in the solar cells was also maximized. Since there is a mismatch between the optical permittivities of the PMLID constituents and the solar cell, reflection occurs at the PMLID/c-Si interfaces. If this reflection could be reduced, the conversion of photonic energy to electrical energy would be further enhanced.



Therefore, we decided to investigate the effect of an isotropic dielectric buffer layer inserted between the PMLID material and the solar cell in an effort to maximize the transfer of optical energy from the PMLID material to the solar cell. Based upon the optical permittivities of the layers in PMLID material and of the semiconductor, this buffer layer should act as an antireflection coating.

Figure 1 presents the schematic of one unit cell of the light-harvesting structure in the xz plane, the structure being invariant along the y axis. At the bottom is a metal grating of period L along the x axis. Atop one period of the metal grating sits a solar cell, atop N_c consecutive periods of the grating sits a PMLID material with N_d periods in the vertical direction, and one period each on both sides of the solar cell are shared by the PMLID material and the buffer layer. The topmost layer is indium-tin oxide (ITO) functioning as an optically transparent electrode. Using data on an optimized PMLID material,² our objective here is to optimize the thickness L_b and the refractive index n_b of the buffer layer, when the solar cell is made of either c-Si or gallium arsenide (GaAs).

The plan of this paper is as follows. Section II provides a brief description of the theory used to compute the specular and non-specular reflectances and transmittances of the light-harvesting structure shown in Fig. 1, when it is illuminated by a linearly polarized plane wave whose propagation vector lies wholly in the xz plane. An $\exp(-i\omega t)$ dependence on time t is implicit, with ω as the angular frequency and $i = \sqrt{-1}$. The spectrally averaged EHP density is calculated using the computed solution. Section III presents numerical results, when the solar cell is made of either c-Si or GaAs. The paper concludes with a few remarks in Sec. IV.

II. THEORY IN BRIEF

A. Geometry

Figure 1 shows the unit cell of the concentrator $\{x \in (0, N_c L + 3L), z \in (-L_o, L_t)\}$, where $L_t = L_d + L_g + L_m$. The region $z < -L_o$ is vacuous, while the top layer $\{x \in (0, N_c L + 3L), z \in (-L_o, 0)\}$ is made of indium-tin oxide.

The PMLID material occupies the regions $\{x \in (0, N_c L + L - L_b), z \in (0, L_d)\}$ and $\{x \in (N_c L + 2L + L_b, N_c L + 3L), z \in (0, L_d)\}$. This material has continuous spans of $(N_c + 2)L - 2L_b = N_c L - 2L_b$ along the x axis periodically. Furthermore, this material has $N_d \geq 1$ periods along the z axis.

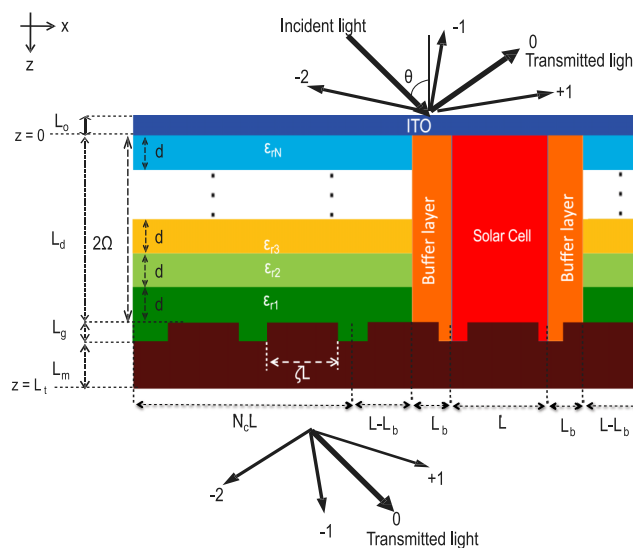


FIG. 1. Schematic of one period (along the x axis) of the light-harvesting structure. When a plane wave is incident at an angle θ with respect to the z axis, the reflected and the transmitted fields comprise specular components (labeled 0) and nonspecular components (labeled $\pm 1, \pm 2, \dots$). A buffer layer is inserted between the PMLID material and the solar cell. The PMLID material is shown to have only one period along the z axis (i.e., $N_d = 1$).

Each period is of thickness $2\Omega = L_d/N_d$ and comprises N layers of equal thicknesses $d = 2\Omega/N$. The relative permittivity $\varepsilon_{rj} > 1$ of the j -th layer, $j \in [1, N]$, is taken to be a real-valued function of the free-space wavelength λ_0 . Our interest lies in the spectral regime $\lambda_0 \in [\lambda_{0min}, \lambda_{0max}]$ dictated by the solar spectrum.

The regions $\{x \in (0, N_c L + L - L_b), z \in (L_d, L_t)\}$ and $\{x \in (N_c L + 2L + L_b, N_c L + 3L), z \in (L_d, L_t)\}$ are occupied by a metallic surface-relief grating with its troughs filled by a dielectric material of relative permittivity ε_{r1} . The metal/dielectric interface has a periodic rectangular profile with a period L along the x axis, corrugation height L_g , and duty cycle $\zeta \in [0, 1]$. The λ_0 -dependent relative permittivity of the metal is denoted by ε_m with $\text{Re}(\varepsilon_m) < 0$ and $\text{Im}(\varepsilon_m) > 0$.

The regions $\{x \in (N_c L + L, N_c L + 2L), z \in (0, L_d)\}$, $\{x \in (N_c L + L, N_c L + 1.5L - 0.5\zeta L), z \in (L_d, L_d + L_g)\}$, and $\{x \in (N_c L + 1.5L + 0.5\zeta L, N_c L + 2L), z \in (L_d, L_d + L_g)\}$ are occupied by a semiconductor of λ_0 -dependent relative permittivity ε_s with $\text{Re}(\varepsilon_s) > 0$ and $\text{Im}(\varepsilon_s) > 0$.

The regions $\{x \in (N_c L + L - L_b, N_c L + L), z \in (0, L_d)\}$, $\{x \in (N_c L + 2L, N_c L + 2L + L_b), z \in (0, L_d)\}$, $\{x \in (N_c L + 0.5L + 0.5\zeta L, N_c L + L), z \in (L_d, L_d + L_g)\}$, and $\{x \in (N_c L + 2L, N_c L + 2.5L - 0.5\zeta L), z \in (L_d, L_d + L_g)\}$ are occupied by a buffer material of relative permittivity $\varepsilon_b = n_b^2 > 1$, which is taken to be non-dissipative and non-dispersive in the spectral regime of interest.

The remainder of the unit cell is occupied by a metal of relative permittivity ε_m . The half space $z > L_t$ is vacuum.

B. Plane-wave response

Suppose that the light-harvesting structure is illuminated by an obliquely incident plane wave whose electric field phasor is given by

$$\mathbf{E}_{inc}(x, z, \lambda_0) = [a_s \hat{\mathbf{u}}_y + a_p (-\hat{\mathbf{u}}_x \cos \theta + \hat{\mathbf{u}}_z \sin \theta)] \exp \{ik_0 [x \sin \theta + (z + L_o) \cos \theta]\}$$

for $z \leq -L_o$. Here and hereafter, θ is the angle of incidence with respect to the z axis, a_s is the amplitude of the s -polarized component, a_p is the amplitude of the p -polarized component, $k_0 = \omega/c_0 = 2\pi/\lambda_0$ is the free-space wavenumber, $c_0 = 1/\sqrt{\varepsilon_0 \mu_0}$ is the speed of light in free space, $\eta_0 = \sqrt{\mu_0/\varepsilon_0}$ is the intrinsic impedance of free space, ε_0 is the permittivity and μ_0 is the permeability of free space, and $\{\hat{\mathbf{u}}_x, \hat{\mathbf{u}}_y, \hat{\mathbf{u}}_z\}$ is the triplet of Cartesian unit vectors.

As depolarization cannot occur in this problem, the electric field phasors of the reflected and the transmitted fields can be stated as^{7,8}

$$\mathbf{E}_{ref}(x, z, \lambda_0) = \sum_{n \in \mathbb{Z}} (a_s r_{ss}^{(n)} \hat{\mathbf{u}}_y + a_p r_{pp}^{(n)} \mathbf{p}_n^-) \exp \{i [\kappa^{(n)} x - \alpha^{(n)} (z + L_o)]\}, \quad z < -L_o, \quad (1)$$

and

$$\mathbf{E}_{tr}(x, z, \lambda_0) = \sum_{n \in \mathbb{Z}} (a_s t_{ss}^{(n)} \hat{\mathbf{u}}_y + a_p t_{pp}^{(n)} \mathbf{p}_n^+) \exp \{i [\kappa^{(n)} x + \alpha^{(n)} (z - L_t)]\}, \quad z > L_t, \quad (2)$$

respectively, where $\mathbb{Z} \equiv \{0, \pm 1, \pm 2, \dots\}$,

$$\kappa^{(n)} = k_0 \sin \theta + 2\pi \frac{n}{(N_c + 3)L}, \quad (3)$$

$$\alpha^{(n)} = \begin{cases} +\sqrt{k_0^2 - (\kappa^{(n)})^2}, & k_0^2 \geq (\kappa^{(n)})^2 \\ +i\sqrt{(\kappa^{(n)})^2 - k_0^2}, & k_0^2 < (\kappa^{(n)})^2 \end{cases}, \quad (4)$$

and

$$\mathbf{p}_n^\pm = \mp \frac{\alpha^{(n)}}{k_0} \hat{\mathbf{u}}_x + \frac{\kappa^{(n)}}{k_0} \hat{\mathbf{u}}_z. \quad (5)$$

The λ_0 -dependent reflection coefficients of order n are denoted by $r_{ss}^{(n)}$ and $r_{pp}^{(n)}$, and the corresponding transmission coefficients by $t_{ss}^{(n)}$ and $t_{pp}^{(n)}$. Thus, the reflected and the transmitted field phasors comprise specular components identified by $n = 0$ and non-specular components identified by $n \neq 0$. Provided that L_m is sufficiently thick, the transmitted field will transport virtually no energy in the $+z$ direction.

In the region $z \in (-L_o, L_t)$, the electric and magnetic field phasors must satisfy the frequency-domain Maxwell curl equations

$$\left. \begin{aligned} \nabla \times \mathbf{E}(x, z, \lambda_0) &= i\omega\mu_0\mathbf{H}(x, z, \lambda_0) \\ \nabla \times \mathbf{H}(x, z, \lambda_0) &= -i\omega\varepsilon_0\varepsilon_r(x, z, \lambda_0)\mathbf{E}(x, z, \lambda_0) \end{aligned} \right\}. \quad (6)$$

We used the finite-element method (FEM)^{9,10} to solve Eqs. (6). After decoupling the s - and p -polarization states and exploiting the independence of the field phasors from y , we reduced Eqs. (6) to two scalar Helmholtz equations, one for each of the two linear polarization states. The boundary conditions on the sides $x = 0$ and $x = N_cL + 3L$ of the unit cell have to be quasi-periodic. Standard transmission conditions hold across the top boundary $z = -L_o$ and bottom boundary $z = L_t$, whose satisfaction involves Eqs. (1)–(2).

We used a special-purpose finite-element meshing function based on the TRIANGLE library.¹¹ Inside each triangle of the mesh, the field phasors were approximated by cubic polynomials. The summations in the expressions of the reflected and transmitted field phasors were truncated to $n \in \{-M_t, M_t\}$.

C. Spectrally averaged EHP density

After obtaining the reflection and transmission coefficients for any $\lambda_0 \in [\lambda_{0min}, \lambda_{0max}]$, the electric field phasor $\mathbf{E}(x, z, \lambda_0)$ can be obtained at any location inside the unit cell, for an unpolarized incident plane wave ($a_s = a_p = E_o/\sqrt{2}$) with an electric field of magnitude $E_o = 1 \text{ V m}^{-1}$.

Thereafter, the spectrally averaged EHP density can be computed as²

$$N_{avg} = \int_{\lambda_{0min}}^{\lambda_{0max}} F(\lambda_0) d\lambda_0, \quad (7)$$

where

$$F(\lambda_0) = \frac{S(\lambda_0) \text{Im}[\varepsilon_s(\lambda_0)]}{LL_d c_0 \hbar E_o^2 \cos \theta} \left\{ \int_{x=N_cL+L}^{N_cL+2L} \left[\int_{z=0}^{z_m(x)} |\mathbf{E}(x, z, \lambda_0)|^2 dz \right] dx \right\}, \quad (8)$$

$$z_m(x) = \begin{cases} L_d + L_g, & x \in (N_cL + L, \\ & N_cL + 1.5L - 0.5\zeta L) \\ L_d, & x \in (N_cL + 1.5L - 0.5\zeta L, \\ & N_cL + 1.5L + 0.5\zeta L) \\ L_d + L_g, & x \in (N_cL + 1.5L + 0.5\zeta L, \\ & N_cL + 2L) \end{cases}, \quad (9)$$

\hbar is the reduced Planck constant, $S(\lambda_0)$ is the AM1.5 solar spectrum,¹² $\lambda_{0min} = 400 \text{ nm}$, and $\lambda_{0max} = 1000 \text{ nm}$.

III. NUMERICAL RESULTS

For all calculations, we set $L_o = 100 \text{ nm}$, a practical value. Also, we chose the metal to be silver and $L_m = 40 \text{ nm}$, and we used measured data for ε_m as a function of λ_0 available elsewhere.¹³

As optimization of the POC alone had previously² provided the relative permittivities of all $N = 9$ layers in every period of the PMLID material, we used the same method here as well. The measured values of the relative permittivity of silicon oxynitrides of 9 different compositions¹³ for $\lambda_0 \in [400, 1000]$ nm were chosen for ε_{rj} , $j \in [1, N]$. Finally, we fixed $L = 400$ nm, consistently with the exploitation of Floquet theory to excite surface-plasmon-polariton waves^{14–16} and waveguide modes.^{16,17}

A. Optimization of POC without buffer layer

We began by assuming that the indium-tin-oxide layer, the buffer layer, and the solar cell are absent. The PMLID material was taken to have $N_d = 3$ periods along the z axis, and that the relative permittivities ε_{rj} from Ref. 13 were changed to $(1 + \delta)^2 \varepsilon_{rj}$, $\delta \in [-0.25, 0.25]$ for all $j \in [1, N]$. We then calculated the solar-spectrum-integrated power-flux density

$$q_0 = \frac{2\eta_0}{L_d} \int_{\lambda_{0min}}^{\lambda_{0max}} S(\lambda_0) \left[\int_0^{L_d} \frac{|P_x(0, z; \lambda_0)|}{E_o^2} dz \right] d\lambda_0, \quad (10)$$

in the plane $x = 0$, as a function of θ , d , ζ , L_g , and δ , when an unpolarized plane wave is incident on the structure. Here, $P_x(x, z; \lambda_0)$ is the x -directed component of the monochromatic time-averaged Poynting vector $\mathbf{P}(x, z; \lambda_0)$. Our experience was that optimization of q_0 in any other plane parallel to $x = 0$ is equally effective.²

Maximization of q_0 was carried out using the differential equation algorithm,¹⁸ while ensuring that a variation of up to 5% in any parameter does not result in a change in q_0 by more than 10%. This modified DEA is designed to avoid any sharp resonances that are either of numerical origin or are physical but would require high-precision manufacturing steps. The following practical design of the POC alone emerged: $\theta = 18$ deg, $d = 130$ nm, $\zeta = 0.75$, $L_g = 40$ nm, and $\delta = 0.25$. This design delivered $q_0 = 4.17 \times 10^3$ W m⁻².

Next, both the indium-tin-oxide layer and the solar cell made of c-Si¹⁹ were considered along with the POC, the buffer layer still being absent. Since $L_b = 0$, the POC has a period of $\tilde{N}_c L$ along the x axis, where $\tilde{N}_c = N_c + 2$. When $\tilde{N}_c = 0$ (i.e., $N_c = -2$), the POC is absent and only the solar cell is present in the unit cell. Only the integer \tilde{N}_c was kept variable, and values $N_{avg}^{(\tilde{N}_c)}$ of the spectrally averaged EHP density N_{avg} were calculated for $\tilde{N}_c \in [0, 4]$. The calculated data are presented in Table I. Clearly, $N_{avg}^{(\tilde{N}_c)}$ increases with \tilde{N}_c , but \tilde{N}_c cannot be too large in a practical situation. As $N_{avg}^{(2)}$ is double of $N_{avg}^{(0)}$ but $N_{avg}^{(3)}$ is not triple of $N_{avg}^{(0)}$, $\tilde{N}_c = 2$ is a practical choice. Significantly, the replacement of two thirds of a solar cell by the POC ($\tilde{N}_c = 2$) results in only about ~ 25% loss of efficiency.

Similar results were found when the solar cell is made of GaAs,²⁰ as Table II shows. However, in this case, the replacement of two thirds of a solar cell by the POC results in only about ~ 10% loss of efficiency.

B. Optimization of buffer layer

Next, in order to determine the optimal buffer layer, we fixed $\theta = 18$ deg, $d = 130$ nm, $\zeta = 0.75$, $L_g = 40$ nm, $\delta = 0.25$, $N_d = 3$, $L = 400$ nm and $L_o = 100$ nm. Our objective was to

TABLE I. Values $N_{avg}^{(\tilde{N}_c)}$ of the spectrally averaged EHP density N_{avg} in relation to \tilde{N}_c when the buffer layer is absent (i.e., $L_b = 0$), $\theta = 18$ deg, $d = 130$ nm, $\zeta = 0.75$, $L_g = 40$ nm, $\delta = 0.25$, $L = 400$ nm, and the solar cell is made of c-Si.

\tilde{N}_c	$N_{avg}^{(\tilde{N}_c)}$ (m ⁻³ s ⁻¹)	$1 - (N_{avg}^{(\tilde{N}_c-1)} / N_{avg}^{(\tilde{N}_c)})$	$N_{avg}^{(\tilde{N}_c)} / N_{avg}^{(0)}$
0	6.82×10^{26}	–	1.00
1	1.32×10^{27}	0.48	1.93
2	1.54×10^{27}	0.14	2.26
3	1.67×10^{27}	0.08	2.45
4	1.74×10^{27}	0.04	2.55

TABLE II. Same as Table I, but the solar cell is made of GaAs.

\tilde{N}_c	$N_{avg}^{(\tilde{N}_c)}$ ($\text{m}^{-3} \text{s}^{-1}$)	$1 - (N_{avg}^{(\tilde{N}_c-1)} / N_{avg}^{(\tilde{N}_c)})$	$N_{avg}^{(\tilde{N}_c)} / N_{avg}^{(0)}$
0	8.30×10^{26}	–	1.00
1	1.71×10^{27}	0.51	2.02
2	2.25×10^{27}	0.24	2.71
3	2.54×10^{27}	0.11	3.06
4	2.72×10^{27}	0.07	3.28

determine the combination $\{L_b, n_b\}$ that maximizes N_{avg} when the solar cell is made of either c-Si or GaAs.²⁰ We also fixed $N_c = 2$ in order to always have at least two periods of POC in all the simulations. Hence, the POC's continuous spans along the x axis would decrease from $4L$ to $2L$ as L_b would increase from 0 to L .

Figure 2 shows the mesh used when $N_d = 1$. The mesh has 27360 triangles in the region $\{x \in [0, L], z \in [-L_o, L_t]\}$ (and in every other similar region of the unit cell), and each triangle is completely filled by just one dielectric material. We set $M_t = 20$ so that the truncation error for

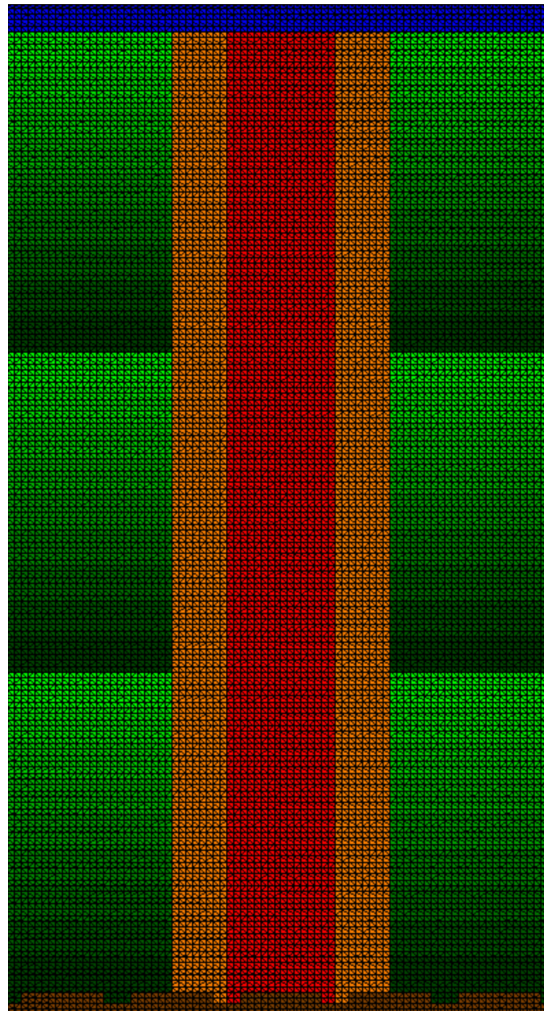


FIG. 2. FEM mesh (dark lines) of the light-harvesting structure. Colors in the background correspond to different regions: Metallic grating (brown), solar cell (red), buffer layer (orange), the PMLID material with $N_d = 3$ (green), and the ITO layer (blue).

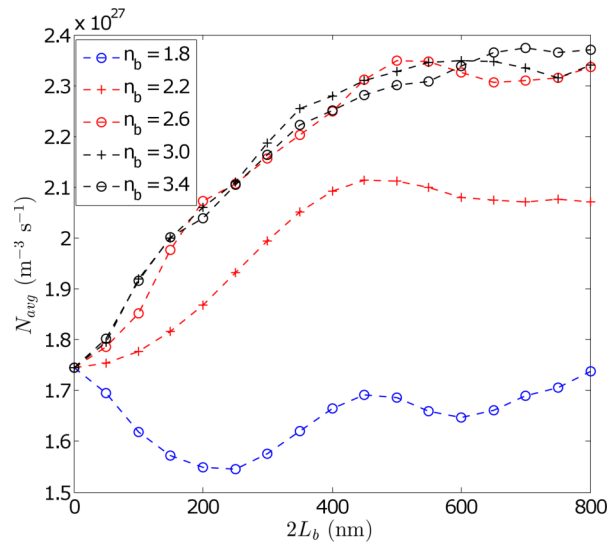


FIG. 3. N_{avg} ($\text{m}^{-3} \text{s}^{-1}$) versus $2L_b$ for $n_b \in \{1.8, 2.2, 2.6, 3.0, 3.4\}$ when the solar cell is made of c-Si, $N_c = 2$, $N_d = 3$, and $n_b = 1.8$ (blue circles), 2.2 (red crosses), 2.6 (red circles), 3.0 (black crosses), or 3.4 (black circles).

the transmitted and reflected waves would be negligible in comparison to the error inherent in partitioning space into triangles, as required by the FEM.

1. c-Si solar cell

Let us first present results for the solar cell made of c-Si, whose relative permittivity as a function of λ_0 is available in the literature.¹⁹

In Fig. 3 the computed values of N_{avg} for $2L_b \in \{0, 50, 100, 150, 200, 250, 300, 350, 400, 450, 500, 650, 700, 750, 800\}$ nm and $n_b \in \{1.8, 2.2, 2.6, 3.0, 3.4\}$ are displayed. The set of values of $2L_b$ was chosen so that the outer edges of the buffer layer always coincide with the mesh lines on the grid.

The spectrally averaged EHP density is always higher if a buffer layer with refractive index larger than 2.2 is present, indicating a reduction in the reflectance at the POC/solar-cell interface. The photon flux in sunlight is maximum at $\lambda_0 \approx 680$ nm,²¹ and the average volume-averaged refractive index of the PMLID material (with refractive indices $(1 + \delta)\sqrt{\epsilon_{rj}} = 1.25\sqrt{\epsilon_{rj}}$, $j \in [1, N]$) at the same wavelength equals 2.1. Since the real part of the refractive index of c-Si is 3.8 at the same wavelength, and the refractive indices of all materials involved are higher for $\lambda_0 < 680$ nm but are weakly dependent on λ_0 for $\lambda_0 > 680$ nm, having $n_b \lesssim 2.1$ is unfruitful for enhancing N_{avg} .

In addition, N_{avg} achieves a maximum at some $2L_b \in [500, 800]$ nm and does not seem to significantly change with further increase in $2L_b$ in Fig. 3. Taking the highest value of N_{avg} from this figure, we concluded that the optimal parameters of the buffer layer are: $2L_b^{opt} = 700$ nm and $n_b^{opt} = 3.4$. Then, $N_{avg}^{opt} = 2.37 \times 10^{27} \text{ m}^{-3} \text{ s}^{-1}$ which is 36% higher than when there is no buffer layer (i.e., $2L_b = 0$).

Let us denote by F^{opt} and F^{ref} the values of F when the buffer layer is optimal (i.e., $2L_b = 700$ nm and $n_b = 3.4$) and absent (i.e., $2L_b = 0$), respectively. Figure 4 shows F^{opt} and F^{ref} as functions of λ_0 . In much of the spectral regime of interest, $F^{opt} > F^{ref}$. The maximum value of the ratio F^{opt}/F^{ref} is 3.50, which occurs for $\lambda_0 = 909.15$ nm.

In Fig. 5, we present the spatial distributions of $|\mathbf{E}(x, z, \lambda_0)|^2$ in the entire structure for $2L_b \in \{0, 200, 450, 800\}$ nm, when $\lambda_0 = 909.15$ nm and $n_b = 3.4$. A band of hot spots occurs in the POC, the buffer layer, and the solar cell when $2L_b = 700$ nm. This band explains the enhancement of F by the insertion of the optimal buffer layer. We attribute the occurrence of such bands to the excitation of (i) surface-plasmon-polariton (SPP) waves whose electric fields are maximal some distance away from the metal/dielectric interface⁸ and (ii) waveguide modes.¹⁷

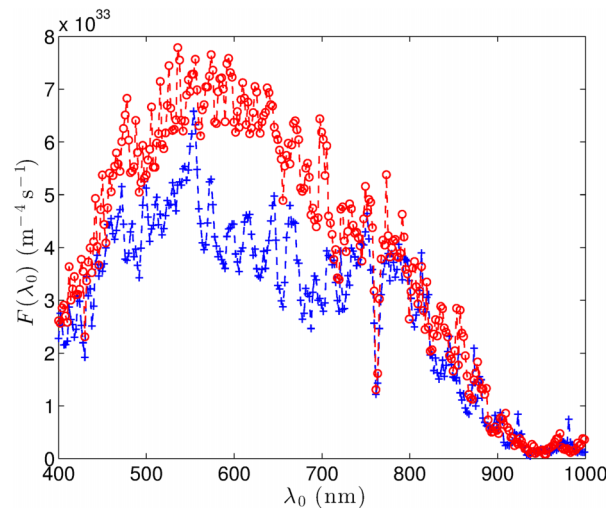


FIG. 4. F^{opt} ($\text{m}^{-4} \text{s}^{-1}$) (red circles) and F^{ref} ($\text{m}^{-4} \text{s}^{-1}$) (blue crosses) versus λ_0 , when the solar cell is made of c-Si.

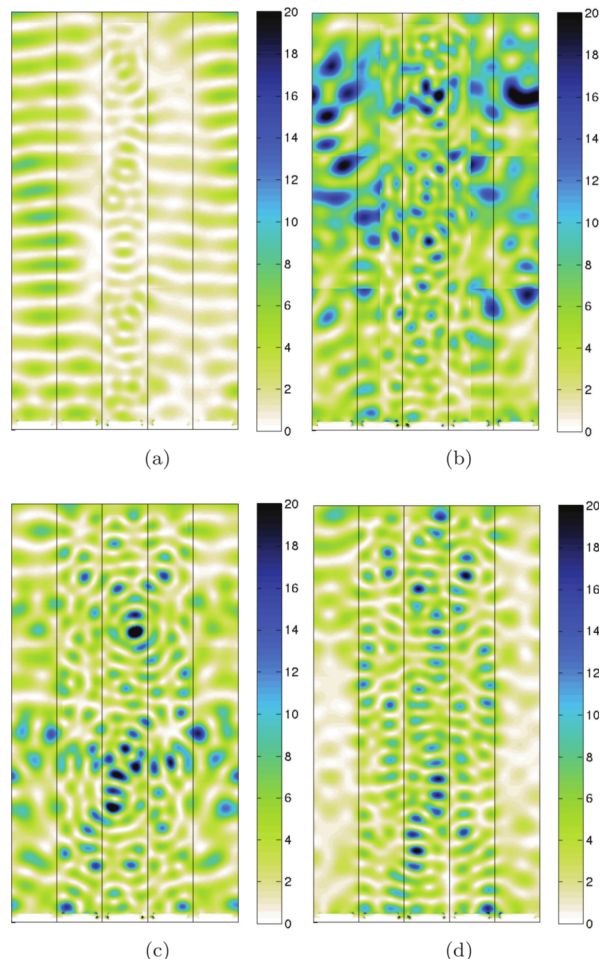


FIG. 5. Spatial distribution of $|\mathbf{E}(x, z, \lambda_0)|^2$ ($\text{V}^2 \text{m}^{-2}$) inside a unit cell of the light-harvesting structure when the incident light is unpolarized, $\lambda_0 = 909.15 \text{ nm}$, the solar cell is made of c-Si, and $n_b = 3.4$. (a) $2L_b = 0$, (b) $2L_b = 400 \text{ nm}$, (c) $2L_b = 700 \text{ nm}$, and (d) $2L_b = 800 \text{ nm}$.

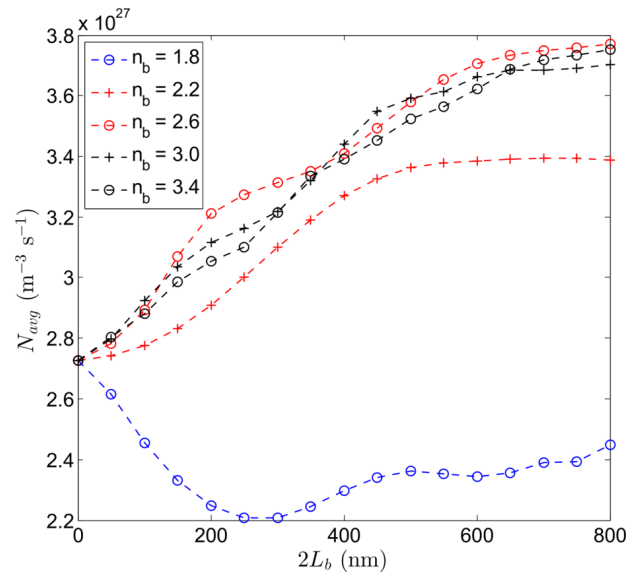
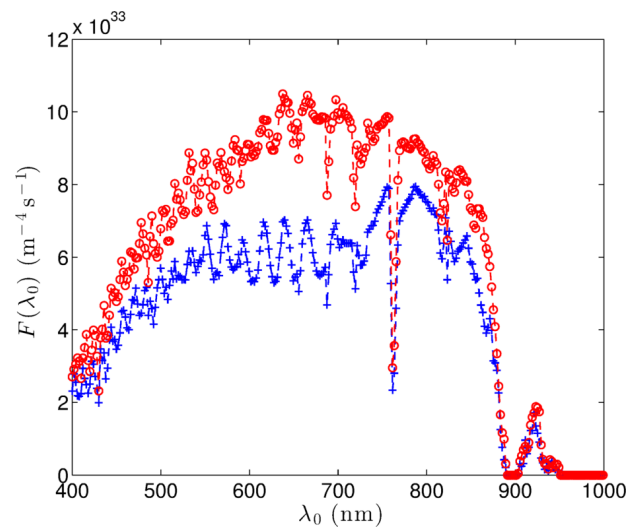


FIG. 6. Same as Fig. 3 but the solar cell is made of GaAs.

Parentetically, when a metal and a homogeneous dielectric material form a planar interface, only one SPP wave can propagate at any given λ_0 .²² Its fields are maximal at the interface and decay exponentially with distance from the interface. When the dielectric material is periodically nonhomogeneous normal to the interface, more than one SPP wave can propagate at any given λ_0 .⁸ These SPP waves differ in phase speed, attenuate rate, degree of localization to the interface, and field profiles. On the dielectric side, some SPP waves have maximal fields at the interface, but others can have maximal fields some distance away from the interface. The significance of multiple SPP waves and multiple waveguide modes excitable at the same value of λ_0 has been experimentally established for the periodically corrugated interface of a metal and a PMLID material.¹⁶

On a per-unit-area basis, replacement of 80% of the solar cell by the the optimal POC will lead to a 49% loss in efficiency. However, replacement of a part of the POC by the optimal buffer layer reduces the efficiency loss to 30%. The use of very cheap dielectric materials for the POC and the buffer layer could offset this reduction.

FIG. 7. F^{opt} ($\text{m}^{-4} \text{s}^{-1}$) (red circles) and F^{ref} ($\text{m}^{-4} \text{s}^{-1}$) (blue crosses) versus λ_0 , when the solar cell is made of GaAs.

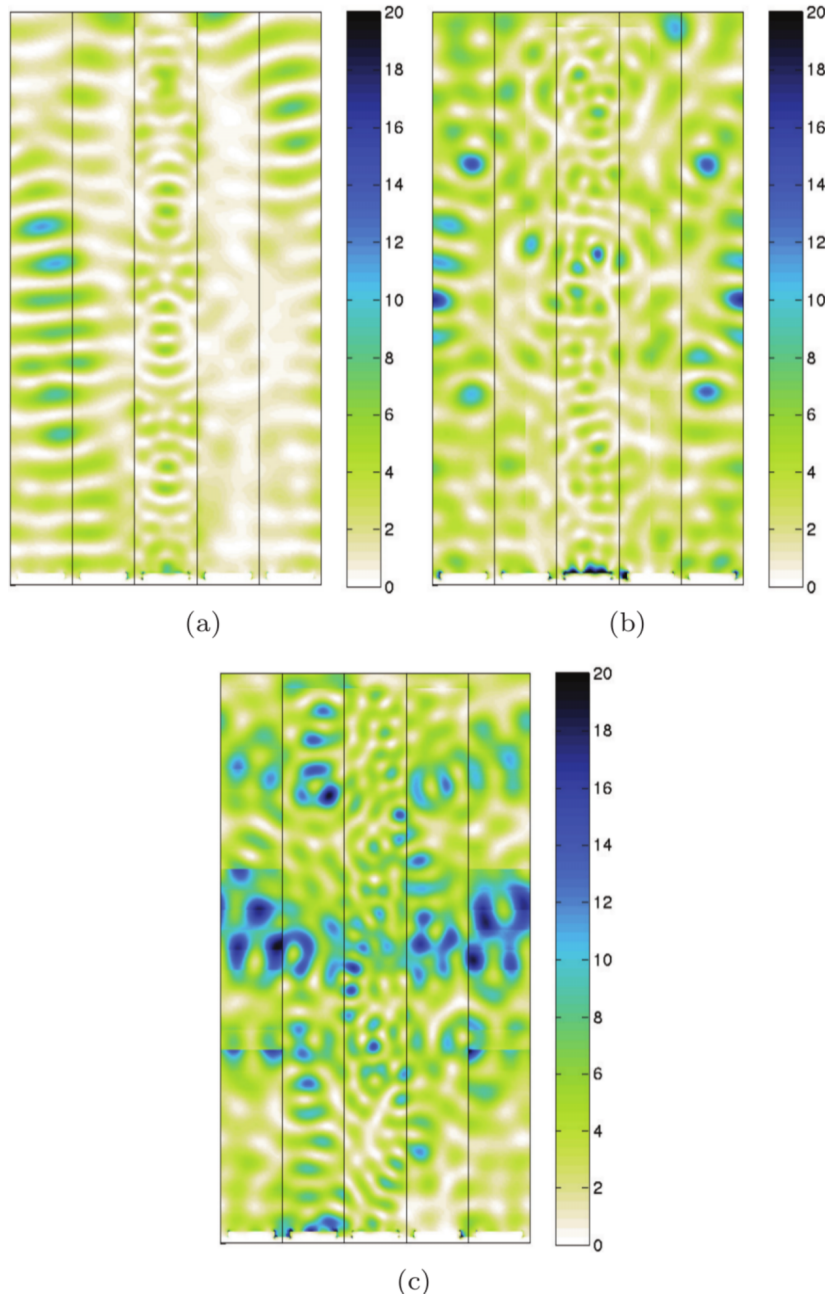


FIG. 8. Spatial distribution of $|\mathbf{E}(x, z, \lambda_0)|^2$ ($\text{V}^2 \text{m}^{-2}$) inside a unit cell of the light-harvesting structure when the incident light is unpolarized, $\lambda_0 = 887.19$ nm, the solar cell is made of GaAs, and $n_b = 2.6$. (a) $2L_b = 0$, (b) $2L_b = 400$ nm, and (c) $2L_b = 800$ nm.

2. GaAs solar cell

The relative permittivity of GaAs as a function of λ_0 was retrieved from a standard resource.²⁰ Let us note here that GaAs has zero conductivity for $\lambda_0 \in [950, 1000]$ nm.

Similarly to Fig. 3, the computed values of N_{avg} versus $2L_b$ and n_b are displayed in Fig. 6. Taking the highest value of N_{avg} from this figure, we concluded that the optimal parameters are: $2L_b^{opt} = 800$ nm and $n_b^{opt} = 2.6$. Then, $N_{avg}^{opt} = 3.77 \times 10^{27} \text{ m}^{-3} \text{ s}^{-1}$ which is 38% higher than when there is no buffer layer (i.e., $2L_b = 0$). Moreover, in Fig. 7 we observe that $F^{opt} > F^{ref}$ for all wavelengths of interest. The maximum value of the ratio F^{opt}/F^{ref} is 2.34, which occurs for $\lambda_0 = 887.19$ nm.

In Fig. 8, we present the spatial distributions of $|\mathbf{E}(x, z, \lambda_0)|^2$ in the entire structure for $2L_b \in \{0, 600, 800\}$ nm, when $\lambda_0 = 909.15$ nm and $n_b = 2.6$. The intensity is higher in the solar cell when the buffer layer is present.

On a per-unit-area basis, replacement of 80% of the solar cell by the combination of the optimal POC and the optimal buffer layer will result in efficiency loss of just 10%. The use of very cheap dielectric materials for the POC and the buffer layer is very likely to offset this reduction.

C. Robustness of the optimal structure

As we were interested in determining the sensitivity of the optimal designs with respect to manufacturing errors, we analyzed the effects on N_{avg} of changes in the shape of the grating.

Perfect rectangular profiles are difficult to realize efficiently in any mass-manufacturing scenario at the nanoscale. Hence, we changed the rectangular shape into trapezoidal by reducing the top dimension of the metal in each unit cell in the region $L_d < L_d + L_g$ from ζL to $(5/6)\zeta L$. This change did not necessitate a significant change in the FEM mesh. The spectrally averaged EHP densities computed with the optimal parameters determined previously in this section are $N_{avg}^{opt} = 2.40 \times 10^{27} \text{ m}^{-3} \text{ s}^{-1}$ (c-Si) and $N_{avg}^{opt} = 3.80 \times 10^{27} \text{ m}^{-3} \text{ s}^{-1}$ (GaAs). These values for the trapezoidal profile differ only by 1.3% (c-Si) and 0.8% (GaAs) with respect to those of N_{avg}^{opt} for the rectangular profile.

We also determined the variation of N_{avg} with respect to $L_g \in [36, 44]$ nm. For $\pm 10\%$ variation of L_g from its optimal value of 40 nm, we found a variation of less than 0.4% in the spectrally averaged EHP density for both c-Si and GaAs cells.

IV. CONCLUDING REMARKS

Given that dielectric materials used in planar optical concentrators are cheaper than photovoltaic materials in common use, the incorporation of a POC can reduce the cost of fabricating solar-cell modules. Our previous work² had shown that a 4:1 POC made of a PMLID material could result in a loss of 48% (on a per-unit-area basis) in efficiency compared to a pure planar solar cell. Our current work improves upon that result through the insertion of a buffer layer between the PMLID material and the solar cell. Our calculations show that the buffer layer can have a wide tolerance in thickness from 250 to 400 nm, which is highly desirable from a manufacturing perspective, and may have a potential optimal thickness in the 350-to-400-nm range. More importantly, the addition of the buffer layer between the PMLID material and the solar cell improves the spectrally averaged electron-hole pair density in a c-Si solar cell by 36% and in a GaAs solar cell by 38% compared to the same structure without the buffer layer for the same solar irradiance conditions.

Relative to a solar-cell module without the POC and the buffer layer, there is an efficiency loss of 30% for c-Si solar cells and 10% for GaAs solar cells accompanied by the combination of the optimal POC and the optimal buffer layer. These losses are amply compensated by the much lower costs of the dielectric materials in comparison to those of the semiconductors.

ACKNOWLEDGMENTS

M. E. Solano acknowledges partial financial support from CONICYT-Chile via grant FONDECYT-11130350 and BASAL project CMM, Universidad de Chile. M. Faryad, G. D. Barber, A. Lakhtakia, and T. E. Mallouk acknowledge partial financial support from US National Science Foundation via grant DMR-1125591 and the research of P. B. Monk is supported in part by DMR-1125590.

¹ G. Kocher-Oberlehner, M. Bardosova, M. Pemble, and B. S. Richards, *Solar Energy Mater. Solar Cells* **104**, 53 (2012).

² M. E. Solano, M. Faryad, P. B. Monk, T. E. Mallouk, and A. Lakhtakia, *Appl. Phys. Lett.* **103**, 191115 (2013); errata: **106**, 079901 (2015).

³ S. Bouchard and S. Thibault, *Opt. Lett.* **39**, 1197 (2014).

⁴ J. Yoon, A. J. Baca, S.-I. Park, P. Elvikis, J. B. Geddes III, L. Li, R. H. Kim, J. Xiao, S. Wang, T.-H. Kim, M. J. Motala, B. Y. Ahn, E. B. Duoss, J. A. Lewis, R. G. Nuzzo, P. M. Ferreira, Y. Huang, A. Rockett, and J. A. Rogers, *Nature Mater.* **7**, 907 (2008).

- ⁵ J. Yoon, L. Li, A. V. Semichaevsky, J. H. Ryu, H. T. Johnson, R. G. Nuzzo, and J. A. Rogers, *Nature Commun.* **2**, 343 (2011).
- ⁶ R. J. Knuesel and H. O. Jacobs, *Adv. Mater.* **23**, 2727 (2011).
- ⁷ J. P. Hugonin, R. Petit, and M. Cadilhac, *J. Opt. Soc. Am.* **71**, 593 (1981).
- ⁸ J. A. Polo, Jr., T. G. Mackay, and A. Lakhtakia, *Electromagnetic Surface Waves: A Modern Perspective* (USA: Elsevier, Waltham, MA, 2013).
- ⁹ P. B. Monk, *Finite Element Methods for Maxwell's Equations* (United Kingdom: Oxford University Press, Oxford, 2003).
- ¹⁰ M. E. Solano, M. Faryad, A. Lakhtakia, and P. B. Monk, *J. Opt. Soc. Am. A* **31**, 2275 (2014).
- ¹¹ <http://www.cs.cmu.edu/~quake/triangle.html> (accessed 27 January 2015).
- ¹² <http://pveducation.org/pvcdrrom/appendices/standard-solar-spectra> (accessed 27 January 2015).
- ¹³ M. Faryad, A. S. Hall, G. D. Barber, T. E. Mallouk, and A. Lakhtakia, *J. Opt. Soc. Am. B* **29**, 704 (2012).
- ¹⁴ L. M. Anderson, *Proc. SPIE* **408**, 172 (1983).
- ¹⁵ P. Sheng, A. N. Bloch, and R. S. Stepleman, *Appl. Phys. Lett.* **43**, 579 (1983).
- ¹⁶ L. Liu, M. Faryad, A. S. Hall, G. D. Barber, S. Erten, T. E. Mallouk, A. Lakhtakia, and T. S. Mayer, *J. Nanophoton.* **9**, 093593 (2015).
- ¹⁷ T. Khaleque and R. Magnusson, *J. Nanophoton.* **8**, 083995 (2014).
- ¹⁸ R. Storn and K. Price, *J. Global Optim.* **11**, 341 (1997).
- ¹⁹ <http://www.filmetrics.com/refractive;index;database/Si/Silicon> (accessed 16 July 2015).
- ²⁰ <http://www.sspectra.com/sopra.html> (accessed 17 July 2015).
- ²¹ M. Chen and R. E. Blankenship, *Trends Plant Sci.* **16**, 427 (2011).
- ²² H. J. Simon, D. E. Mitchell, and J. G. Watson, *Am. J. Phys.* **43**, 630 (1975).